Testing refined shell-model interactions in the *sd* shell: Coulomb excitation of ^{26}Na

B. Siebeck,[1] M. Seidlitz,[1] A. Blazhev,[1] P. Reiter,[1,*] R. Altenkirch,[1] C. Bauer,[2] P. A. Butler,[3] H. De Witte,[4] J. Elseviers,[4] L. P. Gaffney,[4] H. Hess,[1] M. Huyse,[4] T. Kröll,[2,5] R. Lutter,[6] J. Pakarinen,[7,8] N. Pietralla,[2] F. Radeck,[1] M. Scheck,[9,10] D. Schneiders,[1] C. Sotty,[4,11] P. Van Duppen,[4] M. Vermeulen,[12] D. Voulot,[11] N. Warr,[1] and F. Wenander[11]
(for the MINIBALL and REX-ISOLDE Collaborations)
[1]*Institut für Kernphysik, Universität zu Köln, 50937 Köln, Germany*
[2]*Institut für Kernphysik, Technische Universität Darmstadt, 64289 Darmstadt, Germany*
[3]*Oliver Lodge Laboratory, University of Liverpool, Liverpool L69 7ZE, United Kingdom*
[4]*Instituut voor Kern- en Strahlingsfysica, KU Leuven, 3001 Leuven, Belgium*
[5]*Physik Department E12, Technische Universität München, 85748 Garching, Germany*
[6]*Department of Physics, Ludwig Maximilian Universität München, 85748 Garching, Germany*
[7]*Department of Physics, University of Jyväskylä, FI-40014 Jyväskylä, Finland*
[8]*Helsinki Institute of Physics, P.O. Box 64, FI-00014 Helsinki, Finland*
[9]*School of Engineering, University of the West of Scotland, Paisley PA1 2BE, United Kingdom*
[10]*Scottish Universities Physics Alliance, Glasgow G12 8QQ, United Kingdom*
[11]*Physics Department, ISOLDE, CERN, 1211 Geneva 23, Switzerland*
[12]*Nuclear Physics Group, University of York, York YO10 5DD, United Kingdom*
(Received 28 October 2014; revised manuscript received 12 December 2014; published 15 January 2015)

Background: Shell-model calculations crucially depend on the residual interaction used to approximate the nucleon-nucleon interaction. Recent improvements to the empirical *universal sd* interaction (USD) describing nuclei within the *sd* shell yielded two new interactions—USDA and USDB—causing changes in the theoretical description of these nuclei.
Purpose: Transition matrix elements between excited states provide an excellent probe to examine the underlying shell structure. These observables provide a stringent test for the newly derived interactions. The nucleus ^{26}Na with 7 valence neutrons and 3 valence protons outside the doubly-magic ^{16}O core is used as a test case.
Method: A radioactive beam experiment with ^{26}Na ($T_{1/2} = 1{,}07s$) was performed at the REX-ISOLDE facility (CERN) using Coulomb excitation at safe energies below the Coulomb barrier. Scattered particles were detected with an annular Si detector in coincidence with γ rays observed by the segmented MINIBALL array. Coulomb excitation cross sections of the beam have been obtained by normalization to the well known Coulomb excitation cross sections of the ^{104}Pd target.
Results: The observation of three γ-ray transitions in ^{26}Na together with available spectroscopic data allows us to determine $E2$- and $M1$-transitional matrix elements. Results are compared to theoretical predictions.
Conclusion: The improved theoretical description of ^{26}Na could be validated. Remaining discrepancies between experimental data and theoretical predictions indicate the need for future experiments and possibly further theoretical improvements.

DOI: 10.1103/PhysRevC.91.014311 PACS number(s): 21.60.Cs, 23.20.Js, 25.70.De, 29.38.Gj

I. INTRODUCTION

The nuclear shell model provides one of the most established ways to describe properties of atomic nuclei with low or medium masses. Accurate interpretation of experimental findings using *ab initio* no-core shell-model calculations without truncations are only feasible for light nuclei, due to the computational limitations. Thus, with increasing number of nucleons the nucleus will be described by a limited number of valence nucleons outside a doubly-magic core. For those calculations a proper description of the single-particle energies and residual nucleon-nucleon interaction, determining the spectroscopic observables of the nuclei is crucial.

The nucleus studied in this work, ^{26}Na, is part of the *sd* shell, formed of the three single-particle orbitals $1s_{1/2}$, $0d_{3/2}$, and $0d_{5/2}$ for both protons and neutrons outside the doubly-magic core ^{16}O. These valence orbits provide exclusively positive-parity states for all possible configurations. With respect to the available computing power, shell-model calculations in the *sd* shell can be done without truncations of the model space. Restricting the residual interaction in the *sd* shell to two-body forces, a total of 66 parameters are needed to describe the Hamiltonian, i.e., 3 single-particle energies of the valence orbitals and 63 two-body matrix elements for the nucleon-nucleon interaction within these orbits. Therefore, nuclei of the *sd* shell, ranging from ^{16}O up to ^{40}Ca, are ideal test cases for shell-model calculations.

The most common interaction used for shell-model calculations in the *sd* shell is the empirical "universal" *sd* interaction

*Corresponding author: preiter@ikp.uni-koeln.de

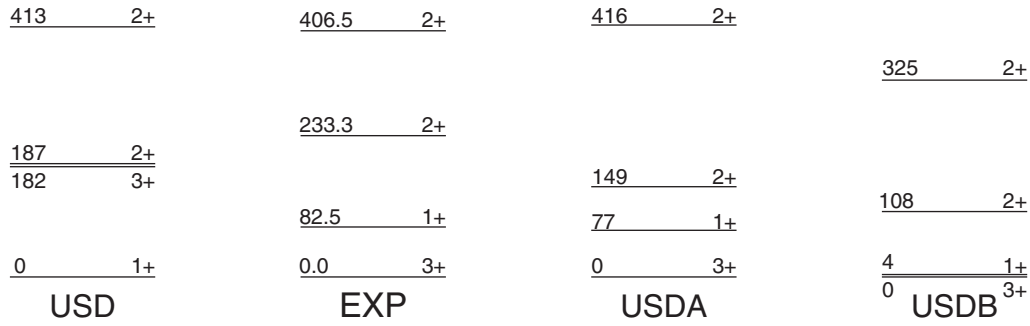

FIG. 1. Comparison between low-lying experimental level energies of ^{26}Na (EXP) from the previously investigated ^{14}C(^{14}C,d)^{26}Na reaction and theoretical predictions using three different interactions (USD, USDA, USDB). The spins of the ground state and the first excited states are correctly reproduced by both new interactions USDA and USDB.

(USD) [1,2]. Here the 66 parameters have been obtained by a fit to 447 experimentally deduced ground-state binding energies and energies of excited states. The fit was executed searching for well-determined uncorrelated linear combinations for the parameters of the Hamiltonian. The original USD interaction has been improved recently by applying the same fit procedure to an extended set of 608 experimental energy data points and making use of improved computing power. In this way two new interactions—USDA and USDB—were obtained [3]. The difference between both interactions is the number of linear combinations, which were varied. For the USDA (USDB) interaction 30 (56) fitted linear combinations were included for the parameters of the Hamiltonian. In both cases the remaining parameters were taken from the renormalized G matrix [4]. Hence, the USDA interaction is closer to the values taken from the G matrix whereas the USDB interaction is the best fit to the experimental data available.

The authors of the USDA/B interactions investigated the reproduction of sd shell observables like magnetic dipole and electric quadrupole moments, transition strengths, as well as GT transition strengths using the new Hamiltonians [5]. A fit for optimal effective charge and effective g-factor values was performed. For nuclei close to stability it was found that the three Hamiltonians yield similar descriptions. Interestingly most of the observables are insensitive to the orbital contribution of $M1$ matrix elements, $E2$ matrix elements, and spectroscopic factors. An exception to this observation are the odd-odd nuclei, ^{30}P and ^{34}Cl, therefore a more complete comparison for odd-odd nuclei was suggested. A low-energy Coulomb excitation study of ^{20}Na provided experimental $B(E2)$ and $B(M1)$ strengths [6] cited to be inconsistent with the USDB calculations. However, different effective charges and effective g factors were used than the values suggested for the USDB interaction [5].

Thus, the predictive power of the USDA/B interactions awaits further verification for odd-odd cases. Already in the original work of Brown and Richter the isobaric chain $A = 26$ was used to point out the improvements in the theoretical description of sd shell nuclei [3]. However, experimental data on excited levels with spin assignments for the neutron-rich odd-odd nucleus ^{26}Na are fairly limited, and the comparison to theory is constrained to the level density and the low-energy part of the level scheme. Recently more experimental data was obtained by investigating the ^{14}C(^{14}C,d)^{26}Na reaction [7].

Calculations using the USD interaction predicted the spin and parity of the ground state and first excited states to be 1^+ and 3^+, respectively. This is in contradiction to the experimentally observed 3^+ ground state [8] and a first excited state with 1^+ at an energy of 82.5 keV [9]. The inversion is resolved by using the new interactions USDA and USDB, both reproducing a level scheme in agreement with experimental data (cf. Fig. 1). Furthermore the USD Hamiltonian predicts four 1^+ states which should be observable in the β decay of ^{26}Ne. Experimentally, only three were observed [10]. Calculations using the new interactions USDA (USDB) result in a $B(GT)$ value of 0.003 (0.008) for one of the ^{26}Ne(0^+) $\rightarrow$ ^{26}Na(1^+) transitions [3], which is too small for the transition to be observed in experiments up to now. Those differences between calculations using the USD interaction and calculations using the USDA or USDB interactions demonstrate the improvement in the theoretical description of ^{26}Na. To probe the new interactions further, transition strengths provide an even more sensitive test for the underlying shell structure. This motivated a Coulomb excitation experiment employing a radioactive ^{26}Na beam.

II. EXPERIMENTAL SETUP AND DATA ANALYSIS

The Coulomb excitation experiment of ^{26}Na was performed at the REX-ISOLDE facility at CERN [11,12]. The radioactive ^{26}Na beam was produced by bombarding an approximately 50-g/cm^2-thick UC$_x$ primary target with 1.4 GeV protons, provided by the CERN PS Booster, at an average proton current of 1.5 μA. Following surface ionization on a hot tungsten surface the produced Na ions were mass separated by the ISOLDE General Purpose Separator. At REX-ISOLDE the ions were first accumulated, cooled, and bunched in a Penning trap before being injected into an electron-beam ion source (EBIS) [13]. In the REXEBIS the ions were charge bred to high charge states. The trap accumulation and charge breeding times were set to 20 and 12 ms, respectively. For post-acceleration only ions with $A/q = 4.33$ (for ^{26}Na $q = 6+$) were selected by an A/q separator. The overall efficiency of the trap-EBIS combination amounts to 12.5%. The radioactive beam was post-accelerated by the REX linear accelerator and

delivered with a final beam energy of 2.82 MeV/nucleon onto the secondary target inside the highly-efficient MINIBALL setup [14]. The average intensity of the post-accelerated ^{26}Na beam amounted to $6.4(5) \times 10^4$ ions/s. During the Coulomb excitation experiment an enriched ^{104}Pd secondary target with a thickness of 3.6 mg/cm^2 was irradiated for 73 h.

Scattered projectile nuclei were detected by an annular 500-μm-thick, double-sided silicon strip detector (DSSSD), consisting of four identical quadrants [14,15]. Each quadrant comprised 16 annular strips at the front side and 12 pairs of sector strips at the back side for identification and reconstruction of the trajectories of the scattered nuclei. Calibration of all DSSSD segments was performed with an α source and data from elastic scattering of ^{13}C on the ^{104}Pd target. The detector covered forward angles between 16.8° and 53.7° in the laboratory system. Deexcitation γ rays following Coulomb excitation of projectile and target nuclei were detected by the MINIBALL γ-ray spectrometer. The MINIBALL spectrometer consists of eight triple cluster detectors in close geometry, each containing three sixfold segmented high purity germanium (HPGe) crystals [14,16]. All MINIBALL detectors were calibrated using ^{60}Co, ^{133}Ba, and ^{152}Eu sources, mounted at target position. The total photo peak efficiency of the array at 1.3 MeV was 8.4(2)% after the add-back procedure was applied, i.e., coincident signals of the three detectors of a MINIBALL cluster were combined. An angle-calibration measurement was performed using Doppler-shifted γ rays after the neutron pick-up reaction ^{22}Ne$(d,p)^{23}$Ne, to determine all angles of the cluster detectors exactly. The high segmentation of the setup ensured a proper Doppler correction for in-flight γ-ray emission at $v/c \sim 8\%$ by combining the angular information of the γ ray with the direction and velocity of the scattered beam particle that was detected in coincidence. Data of the Coulomb excitation measurements were recorded using prompt particle-γ coincidences, i.e., events with a maximum time difference of typically 1 μs between particle and γ ray were registered.

Since all beam nuclei impinging on the target contribute to Coulomb excitation of the target material, which is used for normalization, it was mandatory to investigate possible beam contaminations carefully and to monitor the exact beam composition during the experiment. The beam composition was determined with the help of an ionization chamber, consisting of a CF_4 filled gas cell and a Si detector in succession for the energy loss and residual energy measurements, respectively. The ionization chamber was mounted downstream after the scattering chamber at the beam-dump position. The total accumulated beam composition of the experiment amounted to 42% for ^{26}Na, 54% for ^{13}C, and 4% for other contaminants within a time window of 2.4 s after the proton pulse impact on the primary target. The kinematics of the scattered $A = 26$ ions can be clearly separated from scattered ^{13}C or target ions by the measured correlation of particle energy and scattering angle in the DSSSD. To select the prompt Coulomb excitation events and to suppress random coincidences from room background, i.e., β decay and bremsstrahlung, a time window with a width of $\Delta t_p = 250$ ns was applied for the time difference between the particle and the γ ray. The prompt Coulomb excitation spectrum is particularly clean of any background

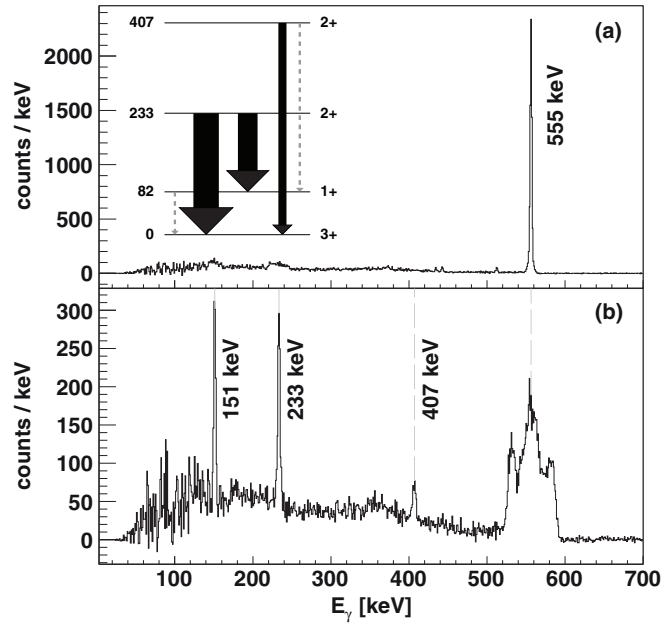

FIG. 2. Background-subtracted energy spectra after Coulomb excitation of ^{26}Na in coincidence with scattered beam particles. The Doppler correction was performed for the ^{104}Pd target (a) and the ^{26}Na beam (b). All observed transitions can be assigned to the known level schemes of ^{104}Pd and ^{26}Na. The inset shows the partial level scheme of ^{26}Na with the transition observed in the present work. The width of the arrows is proportional to the intensity; dashed arrows indicate unobserved transitions.

transitions after background subtraction with a background time window $\Delta t_r = 1000$ ns. All observed γ-ray transitions are due to Coulomb excitation of either $A = 26$ beam or target nuclei. The experimental method follows the procedures given in Ref. [14,17], where additional information can be found.

III. RESULTS

The obtained final γ-ray spectrum is shown in Fig. 2. Two different Doppler corrections are applied in order to extract the yields both for target and projectile nuclei. Due to the given kinematics, ^{104}Pd is scattered into an angular range of 70°–95° in the laboratory frame and is largely stopped inside the target. Therefore only minimal Doppler correction is needed. For the beam-like particles, the velocity is deduced from the deposited energy in the DSSSD. The determination of the relative angle between the hit segment in the DSSSD and in the MINIBALL array allows an excellent Doppler correction. Three in-flight transitions become visible which are assigned to the known level scheme of ^{26}Na. Two low-energy γ-ray transitions were not observed (cf. inset of Fig. 2, dashed lines). The level at 82.5 keV, corresponding to the $1^+ \rightarrow 3^+$ transition, has a rather long half-life of 9(2) μs [18]. This exceeds by far any of the electronic time-gates and therefore this transition was not detected. The other unobserved transition $2_2^+ \rightarrow 1^+$ has a known branching ratio of only 16% [7]. Taking the 240 counts from the corresponding

TABLE I. Observed γ-ray transitions in the Coulomb excitation of ^{26}Na on ^{104}Pd. For details on the correction factors used for the final yields see the text.

Isotope	$I_i \rightarrow I_f$	E_γ lit. (keV)	E_γ (keV)	N_γ (counts)	N_γ cor. (counts)
^{26}Na	$2_1^+ \rightarrow 1^+$	150.9	151(1)	875(35)	3279(131)
^{26}Na	$2_1^+ \rightarrow 3^+$	233.3	233(1)	937(37)	4046(162)
^{26}Na	$2_2^+ \rightarrow 3^+$	406.5	407(2)	240(24)	1374(137)
^{104}Pd	$2_1^+ \rightarrow 0_1^+$	555.796(23)	556(1)	6702(82)	42743(568)

$2_2^+ \rightarrow 3^+$ transition this yields about 40 counts in the spectra [cf. Fig. 2(b)] which is just at the detection limit in the energy range around 324 keV. Transitions from higher-lying states at around 1.5 MeV, known from previous experiments [7,10], were not observed.

The observed transitions are fitted and corrected for energy-dependent γ-ray detection efficiency. Furthermore the target excitation is corrected for excitation coming from beam impurities. The particle gate allows to select the scattering of $A = 26$ nuclei on ^{104}Pd, excluding ^{13}C from the further analysis. The results of the fitted transitions are summarized in Table I.

The coupled channels Coulomb excitation code GOSIA2 [19,20] was used in order to fit transition matrix elements to the experimental data and known spectroscopic data, i.e., branching and multipole mixing ratios [7] and half-lives [18]. GOSIA2 varies the matrix elements until the experimentally observed yields and other known spectroscopic data points are reproduced, taking into account also multistep excitation, reorientation, and angular distributions. The Coulomb excitation of the well-known target nucleus ^{104}Pd was used as normalization for the projectile excitation. For the Pd target 14 matrix elements were fitted to one γ-ray yield and 14 matrix elements known from various previous experiments [21]. For the projectile there are 13 relevant matrix elements and 10 data points, i.e., three γ-ray yields, one lifetime [18], two branching ratios and four multipole mixing ratios [7]. This makes a careful distinction between the impacts of the different parameters crucial. Effects of the magnetic dipole moment ($M1$ diagonal matrix element) can be neglected for this type of Coulomb excitation experiments. The electric quadrupole moment ($E2$ diagonal matrix element) can have a significant impact on the yields. This diagonal matrix element was investigated by a χ^2 hyper-surface scan, where the χ^2 was plotted in dependence of the diagonal matrix element and the matrix element for the corresponding ground-state transition. However, no effect on the χ^2 value for different diagonal matrix elements was observed. Thus, the quadrupole moments of the ground state and both observed 2^+ states were neglected. Consistent results were obtained by an additional calculation constrained to experimental values for both diagonal matrix elements given in Ref. [22,23]. The transition from the first excited state to the ground state has not been observed; the diagonal matrix element of the 3^+ state cannot be inferred. At this point a reduced set of nine parameters has to be fitted.

TABLE II. Experimentally determined $B(\pi\lambda)$ values of ^{26}Na in comparison to theoretical values.

		$1^+ \rightarrow 3^+$	$2_1^+ \rightarrow 3^+$	$2_1^+ \rightarrow 1^+$	$2_2^+ \rightarrow 3^+$
$B(E2)$ (W.u.)	EXP	3.10[a]	12.9^{+14}_{-13}	26^{+67}_{-19}	3.18^{+29}_{-29}
	USD	8.66	6.25	3.09	11.27
	USDA	8.39	10.06	1.23	7.91
	USDB	6.88	10.04	1.84	7.89
$B(M1)$ (W.u.)	EXP		0.128^{+280}_{-67}	0.44^{+73}_{-22}	0.153^{+423}_{-83}
	USD		0.14	0.0002	0.34
	USDA		0.04	0.011	0.34
	USDB		0.07	0.023	0.32

[a]The $B(E2)$ value for the $1^+ \rightarrow 3^+$ transition was determined using the lifetime from Ref. [18] as well as total conversion coefficients from the BRICC code [24].

In order to account for the effects of the poorly determined multipole mixing ratios, two separate fits were performed: First pure $E2$ transitions were assumed. The reduced transition probabilities for this calculation are 12.48 (88.11, 3.78) W.u. for the $2_1^+ \rightarrow 3^+$ ($2_1^+ \rightarrow 1^+$, $2_2^+ \rightarrow 3^+$) transition. The second fit uses the experimental multipole mixing ratios from Ref. [7], i.e., $\delta = -0.32(14)$ $(0.16(7), -0.25(12))$ for the $2_1^+ \rightarrow 3^+$ ($2_1^+ \rightarrow 1^+$, $2_2^+ \rightarrow 3^+$) transition. The results from the second fit are summarized in Table II. The comparison of both fits shows only small deviations of the $E2$ transition strengths, connecting excited states with the ground state. This demonstrates that those matrix elements can be determined quite precisely, as the Coulomb excitation, i.e., the level population after the reaction, strongly depends on these matrix elements. However, the unreasonably large matrix element of the $B(E2; 2_1^+ \rightarrow 1^+)$ transition in the first fit without multipole mixing ratios implies that for the other transitions the multipole mixing ratios are relevant. Therefore fits under the assumption of pure $E2$ transitions are not further investigated and, for all fits described in the following, the multipole mixing ratios from Ref. [7] are used. Hence, the precision of the $B(E2; 2_1^+ \rightarrow 1^+)$ and all $B(M1)$ is dominated by the errors of the multipole mixing ratios.

The method described in Ref. [25] was applied in order to extract values for the matrix elements and the associated uncertainties. One matrix element $\langle \Psi_f || T(\pi\lambda) || \Psi_i \rangle$ is fixed while all other matrix elements can be freely varied during the minimization by GOSIA2. Then the fixed matrix element is varied stepwise and the minimization process is repeated. For each iteration, χ^2 is plotted as function of $\langle \Psi_f || T(\pi\lambda) || \Psi_i \rangle$. The value for the matrix element is then found at the minima $\chi^2_{\min}$ and the 1σ-confidence interval is given by $\langle \Psi_f || T(\pi\lambda) || \Psi_i \rangle \leqslant \chi^2_{\min} + 1$. The plots for all matrix elements are shown in Fig. 3. All graphs show a clear minimum. As the plots are the result of a highly correlated nonlinear minimization process, one has to deal with the appearance of scattered spurious points [cf. Figs. 3(b), 3(d), and 3(f)]. These points are due to numerical effects or a premature termination of the minimization. However, the overall quality of the plots is barely affected by those points. Approximate linearity in the neighborhood of the minimum

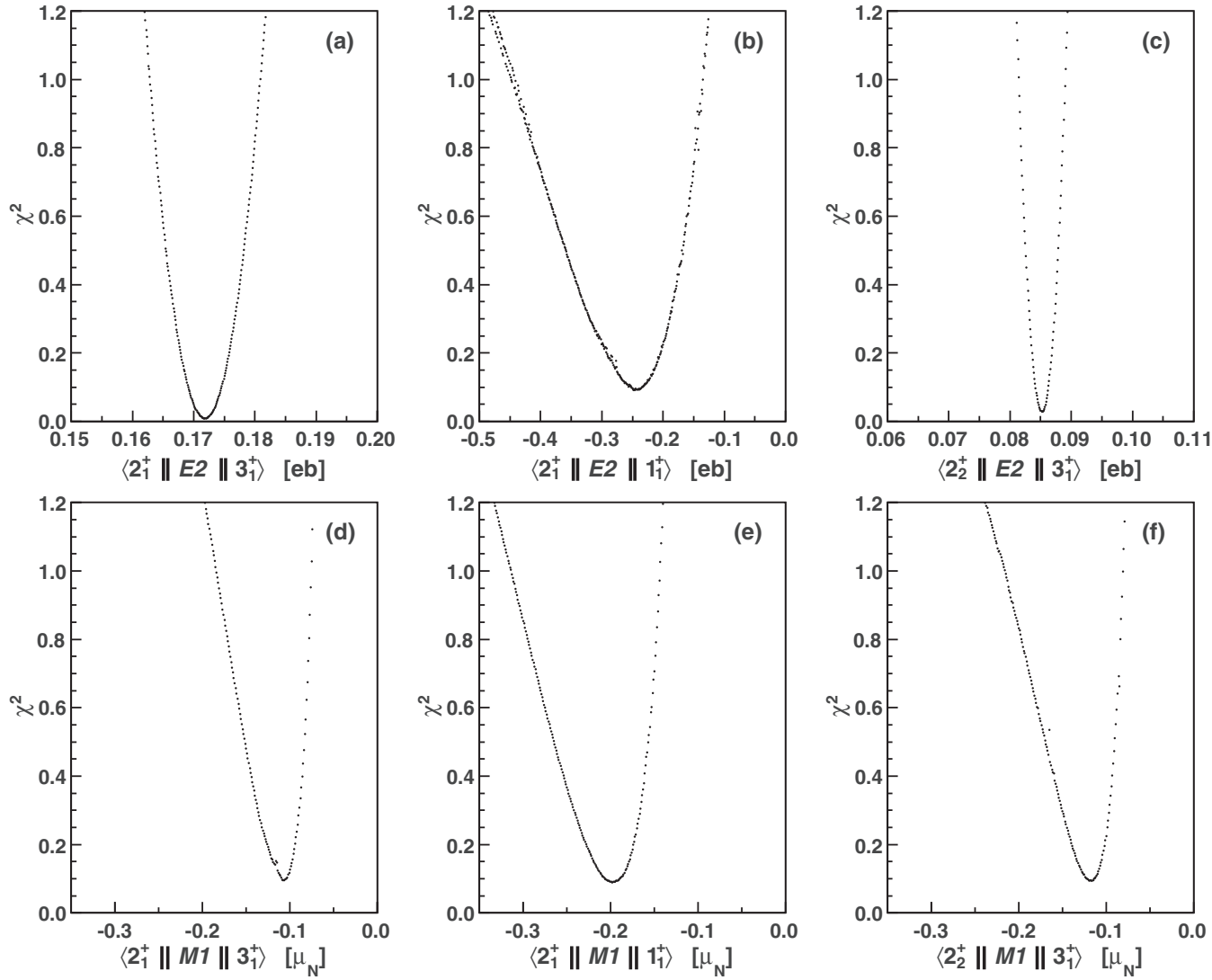

FIG. 3. χ^2-hypersurface scans for all fitted matrix elements. Each point corresponds to a complete GOSIA2 minimization. Please note the different scales on the x axis. The step size for the matrix elements in (a) and (c) is 10^{-4} eb, whereas the step size for all other matrix elements is 10^{-3} eb and $10^{-3}\mu_N$, respectively. More information is given in the text.

is necessary for the method to hold [25]. This condition is perturbed if the matrix element approaches singularity in the multipole mixing ratio at $\langle\Psi_f||M1||\Psi_i\rangle = 0$. In this case the χ^2 is growing rapidly, which leads to an underestimation of the error. Nevertheless, especially for the most relevant matrix elements $\langle 2_1^+||E2||3^+\rangle$ and $\langle 2_2^+||E2||3^+\rangle$ reliable results are obtained, evinced by the parabolic behavior in Figs. 3(a) and 3(c).

IV. DISCUSSION

Coulomb excitation below the Coulomb barrier is dominated by $E2$ excitations. Therefore, $E2$ matrix elements connecting excited states and the ground state can be obtained quite precisely from the measured γ-ray yields. In contrast the determination of $E2$ and $M1$ matrix elements of transitions between excited states strongly depends on the precision of experimentally deduced branching ratios and multipole mixing ratios. Therefore, the following discussion is mainly focused on the $E2$ ground-state transitions.

The reduced transition probabilities of the ground-state transitions of both 2^+ states of ^{26}Na were determined as $B(E2; 2_1^+ \rightarrow 3^+) = 12.9^{+14}_{-13}$ W.u. and $B(E2; 2_2^+ \rightarrow 3^+) = 3.18^{+29}_{-29}$ W.u. These values were compared to shell-model calculations, which were carried out in the sd model space with the USD [1,2], USDA, and USDB [3] Hamiltonians using the codes NUSHELL@MSU [26] and NUSHELLX@MSU [27]. For the calculations, standard values for effective charges, i.e., $e_\pi = 1.35$, $e_\nu = 0.35$, were used, which are close to the values suggested by Ref. [5]. For calculating $M1$ transitions, free nucleon g factors were used.

The experimentally deduced $B(E2)$ values are in reasonable agreement with USDA and USDB calculations that yielded 10.06 and 10.04 W.u. for the deexcitation of the 2_1^+ state and 7.91 and 7.89 W.u. for the deexcitation of the 2_2^+ state, respectively. The theory slightly underestimates

the $B(E2;2_1^+ \rightarrow 3^+)$ and overestimates the $B(E2;2_2^+ \rightarrow 3^+)$. Also the energy splitting of both 2^+ states is larger in the theoretical predictions than experimentally observed, indicating that the mixing of the 2^+ states is overestimated.

The measured values disfavor the USD calculation, which wrongly predicts a larger $B(E2;2_2^+ \rightarrow 3^+)_{\mathrm{USD}} = 11.27$ W.u. than the $B(E2;2_1^+ \rightarrow 3^+)_{\mathrm{USD}} = 6.25$ W.u. These differences between the USD and USDA/B $B(E2;2_i^+ \rightarrow 3^+)$ strengths can be traced back by analyzing the shell-model configurations of the involved states. Shell-model calculations show that for the three different interactions the wave function of the 3^+ state in ^{26}Na is dominated by a $\pi(d_{5/2}^3)_{5/2^+} \otimes \nu(d_{5/2}^6 s_{1/2}^1)_{1/2^+}$ configuration. Configurations containing either an unpaired nucleon in the $\pi s_{1/2}$ orbital or in the $\nu d_{5/2}$ orbital are favored for the 2_1^+ state compared to the 2_2^+ state for the USDA and USDB interactions. Those configurations allow for protons and neutrons equally the so-called stretched $E2$ transitions $(\Delta j, \Delta l = 2)$, caused by one-particle transitions between the $s_{1/2}$ and $d_{5/2}$ orbitals, which contribute most to the total $E2$ transition probabilities. This is reflected in the corresponding differences in the $B(E2;2_i^+ \rightarrow 3^+)$ values. However, due to the extra mixing of the 2_1^+ and 2_2^+ states in the shell-model description, the values differ from the experimental ones, as noticed above. For the USD interaction, however, the important configurations of the two low-lying 2^+ states are interchanged; i.e., the 2_1^+ state contains significantly less $\pi s_{1/2}$ and $\nu d_{5/2}$ configurations in its wave function than the 2_2^+ state.

The measured transition strength between the 2_1^+ and 1^+ state is expected to be dominated by a strong $M1$ component, as the pure $E2$ limit would yield an unreasonably high $B(E2)$ value of 88.11 W.u. Including the multipole mixing ratios given in Ref. [7], the corresponding $E2$ matrix element is reduced drastically. However, the deduced value of $B(E2;2_1^+ \rightarrow 1^+) = 26^{+67}_{-19}$ W.u. also exceeds the shell-model values by one order of magnitude, although with a large uncertainty due to the large error of up to 50% for the multipole-mixing ratios. Indeed all experimentally determined $B(M1)$ values are affected by the imprecisely known multipole-mixing ratios. For this reason we refrained from a detailed comparison with shell-model calculations of $M1$ strengths.

The shell-model calculations with different interactions are compared to known experimental static moments for the ground state of ^{26}Na [22,23]. For the magnetic dipole moment μ_I the changes between the different interactions are very small. The shell-model results for the magnetic dipole moment are $\mu_I = 2.723\,\mu_N$ $(2.635\,\mu_N,\ 2.631\,\mu_N)$ for the USD (USDA, USDB) interaction. They are very similar and slightly smaller than the experimentally obtained value $\mu_I = 2.851(2)\,\mu_N$ from Ref. [23]. For the electric quadrupole moment Q_s the agreement between experiment and calculations using the recent USDA/B interactions is improved with respect to the USD interaction. The USD (USDA, USDB) interaction values for the quadrupole moment $Q_s = -11.27$ mb $(-5.22$ mb, -4.88 mb) compare to the experimental value of $Q_s = -5{,}3(2)$ mb [22]. Together with the inverse spin order of the ground (3^+) and first excited (1^+) state, predicted by the USD interaction, the new results clearly point to the fact that the USD interaction does not reproduce the observed nuclear properties of ^{26}Na. Calculations using the new USDA and USDB interactions show a significant improvement in reproducing the experimental data.

V. SUMMARY

Shell-model calculations in the *sd* shell were recently improved by the two new interactions USDA/USDB and first experimental justification was obtained by comparison to known experimental results for nuclei along the isobaric $A = 26$ chain [3]. A complementary test is provided by comparison with new transition strength values for the unstable odd-odd isotope ^{26}Na, obtained from a Coulomb excitation experiment presented in this work. γ-ray transitions from two of the first three excited states were analyzed and six $B(\pi\lambda)$ values are compared to theoretical values. The $B(E2)$ values for the transitions from the first two excited 2^+ states into the 3^+ ground state are determined with good accuracy. These results clearly show a better agreement between experiment and the new USDA and USDB description and disfavor the use of the older USD interaction. A clear distinction between USDA and USDB based on the transition strengths is not possible; both interactions provide results of similar magnitude. However, together with the values for the excitation energies of the low-lying states the USDA description of ^{26}Na is closer to the known experimental findings.

For a more complete comparison, also other transition strength values should be taken into account. At the moment, however, the experimental values depend crucially on branching ratios and multipole mixing ratios which are not precisely determined, motivating future experiments.

ACKNOWLEDGMENTS

This work has been supported by the German BMBF (Contracts No. 06K-167, No. 06KY205I, No. 05P09PKCI5, and No. 05P12PKFNE), by the European Nuclear Science and Applications Research ENSAR (Project No. 262010), by the Belgian FWO-Vlaanderen, by an FWO Pegasus Marie Curie Fellowship, by GOA/2010/010 (BOF KU Leuven), and by the Interuniversity Attraction Poles Programme initiated by the Belgian Science Policy Office (BriX network P7/12).

[1] B. Wildenthal, Prog. Part. Nucl. Phys. **11**, 5 (1984).
[2] B. A. Brown and B. H. Wildenthal, Annu. Rev. Nucl. Part. Sci. **38**, 29 (1988).
[3] B. A. Brown and W. A. Richter, Phys. Rev. C **74**, 034315 (2006).
[4] M. Hjorth-Jensen, T. T. Kuo, and E. Osnes, Phys. Rep. **261**, 125 (1995).
[5] W. A. Richter, S. Mkhize, and B. A. Brown, Phys. Rev. C **78**, 064302 (2008).
[6] M. A. Schumaker *et al.*, Phys. Rev. C **80**, 044325 (2009).
[7] S. Lee *et al.*, Phys. Rev. C **73**, 044321 (2006).
[8] G. Klotz *et al.*, Nucl. Phys. A **205**, 90 (1973).
[9] K. I. Pearce *et al.*, Phys. Rev. C **35**, 1617 (1987).

[10] L. Weissman *et al.*, Phys. Rev. C **70**, 057306 (2004).
[11] ISOLDE, the ISOLDE facility web page, http://isolde.web.cern.ch (2014).
[12] D. Habs *et al.*, Hyperfine Interact. **129**, 43 (2000).
[13] F. Wenander, 5th International Conference on Radioactive Nuclear Beams [Nucl. Phys. A **701**, 528 (2002)].
[14] N. Warr *et al.*, Eur. Phys. J. A **49**, 40 (2013).
[15] A. Ostrowski *et al.*, Nucl. Instrum. Methods Phys. Res. Sec. A **480**, 448 (2002).
[16] J. Eberth *et al.*, Prog. Part. Nucl. Phys. **46**, 389 (2001).
[17] M. Seidlitz *et al.*, Phys. Rev. C **89**, 024309 (2014).
[18] J. P. Dufour *et al.*, in Nuclei Far From Stability: 5th International Conference, September 1987, Rosseau Lake, Ontario, edited by I. S. Towner, AIP Conf. Proc. No. 164 (AIP, New York, 1988), p. 344.
[19] T. Czosnyka, D. Cline, and C. Y. Wu, Bull. Am. Phys. Soc. **28**, 745 (1983).
[20] T. Czosnyka *et al.*, GOSIA Coulomb excitation codes, manual (University of Rochester, Rochester, NY, 2011).
[21] P. M. Endt, Nucl. Phys. A **633**, 1 (1998).
[22] M. Keim *et al.*, Eur. Phys. J. A **8**, 31 (2000).
[23] G. Huber *et al.*, Phys. Rev. C **18**, 2342 (1978).
[24] T. Kibédi *et al.*, Nucl. Instrum Methods Phys. Res. Sect. A **589**, 202 (2008).
[25] D. Rogers, Nucl. Instrum. Methods **127**, 253 (1975).
[26] B. A. Brown and W. D. M. Rae, NUSHELL@MSU, MSU-NSCL technical report, 2007 (unpublished).
[27] NUSHELLX@MSU, http://www.nscl.msu.edu/∼brown/resources/resources.html (2013).